Correspondence: Lev Ostrovsky (lev.ostrovsky@gmail.com)

Evolution of small-scale turbulence at large Richardson numbers

Lev Ostrovsky[1], Irina Soustova[2], Yuliya Troitskaya[2], and Daria Gladskikh[2,3,4]

[1]Dept. of Applied Mathematics, University of Colorado, Boulder, CO, 80309 USA
[2]Institute of Applied Physics, Russian Academy of Sciences, 603950 Nizhny Novgorod, Russia
[3]Moscow Center for Fundamental and Applied Mathematics, 119991 Moscow, Russia
[4]Research Computing Center, Moscow State University, 119991 Moscow, Russia

Abstract. The theory of stratified turbulent flow developed earlier by the authors is applied to data from different areas of the ocean. It is shown that turbulence can be amplified and supported even at large gradient Richardson numbers. The cause of that is the exchange between kinetic and potential energies of turbulence. Using the profiles of Brunt-Väisälä frequency and vertical current shear given in Forryan et al. (2013), the profiles of kinetic energy dissipation rate are calculated. The results are in reasonable agreement with the experimental data.

1 Introduction

At present, it is well established that the processes in the upper mixed layer of the ocean and inland waters play a significant role both in the development of global climate models and in the creation of regional weather forecast models (e.g., Hostetler et al., 1993; Ljungemyr et al., 1996; Tsuang et al., 2001; Mackay, 2006). Small-scale and mesoscale processes effectively interact with each other and provide energy sink for currents and waves of larger scales. Such processes as wind wave breaking, surface and subsurface shear flows can cause turbulent mixing and the resulting fine structure formation with areas of sharp gradients of temperature and salinity. Whereas the mechanisms of generation of small-scale turbulence are understood reasonably well, the problem of its interaction with other types of motions and long-time support is less clear. Earlier works were based on the Miles's instability condition $R_\mathrm{i} < 1/4$, where R_i is the gradient Richardson number. However, in many observations, turbulence exists in a quasi-stationary regime at much larger R_i, up to 10 and more. In some works, it was explained by the presence of fine structure of current, with thin layers of strong shear (Smyth et al., 2013). A more general description is based on the semi-empirical $K-\varepsilon$ equations (Burchard, 2002; Burchard and Bolding, 2002; Mellor and Yamada, 1982) showing that the developed turbulence can be amplified and supported under a softer condition $R_\mathrm{i} < 1$ (Monin and Yaglom, 1964). Similar equations were used in more specific models of formation of the upper turbulent layer (Ostrovsky and Soustova, 1969), and of the action of internal waves on turbulence (Ivanov et al., 1983; Strang and Fernando, 2001; Stretch et al., 2001). However, even that is insufficient to explain many observations in the ocean and atmosphere where the turbulence is observed at significantly larger R_i (Forryan et al., 2013; Avicola et al., 2007; Galperin et al., 2021). New theoretical models have also appeared for describing non-stationary turbulent processes in the atmosphere and ocean. They are based on spectral approach,

confirming, in particular, the absence of a critical Richardson number for describing turbulent-wave processes in a stratified fluid (Sukoriansky et al., 2003, 2005b, a; Galperin and Sukoriansky, 2020; Galperin et al., 2021, 2007).

In Ostrovsky and Troitskaya (1987), within the framework of a kinetic approach, a closed non-stationary model of turbulence interacting with a variable current was suggested. It includes mutual transformation between kinetic and potential energies of turbulence. The latter is associated with the density fluctuations occurring in stratified turbulence (Monin and Ozmidov, 1981). The theory suggested in Ostrovsky and Troitskaya (1987) is based on the equation for the variable probability distribution function of fluid velocity and density. This approach reduces the uncertainty of standard semi-empirical $K-\varepsilon$ schemes and naturally includes the potential energy of turbulence in the model. As a result, small-scale turbulence can be supported at a non-zero level by the average shear at any finite values of the gradient Richardson number, without a threshold. Later this approach was further developed in Zilitinkevich et al. (2007a, b); Soustova et al. (2020) in application to atmospheric turbulence, where the energy and flux budget (EFB) model was added to the theory. The correspondence between this theory and the $K-\varepsilon$ model, as well as the proper parametrization using the turbulent Prandtl number, are discussed in recent works (Gladskikh et al., 2023; Rodi, 1980).

In this paper, the kinetic model of turbulence is used to describe the evolution and structure of the upper turbulent layer with the parameters taken from in situ observations. Particular attention is paid to the cases of the large Richardson number and the role of turbulent potential energy in explaining the observation data. As an example, we use some data from the paper (Forryan et al., 2013) that provided a relatively detailed set of measuremets for three cruises taken in 2006-2009 in different areas of the world ocean: North Atlantic (cruise D3406, June-July 2006, and cruise D321, July - August 2007) and Southern Ocean (cruise JC29, November-December 2008). These experiments were aimed at studying turbulent mixing in the presence of a stratified shear flow associated with mesoscale motions such as eddies and fronts. With the given profiles of current shear and buoyancy frequency taken from Forryan et al. (2013), the theory developed in Ostrovsky and Troitskaya (1987) yields the results that satisfactorily agree with the measurements of the turbulent dissipation rate given in Forryan et al. (2013). The details of measurements can be found in Forryan et al. (2013) and references therein.

2 Basic equations

The general equations obtained in Ostrovsky and Troitskaya (1987), see also Gladskikh et al. (2023), are shown in the Appendix. Here they will be used for the particular case of known profiles of horizontal current shear $\partial\langle u_x\rangle/\partial z = V_z$ where $\langle u_x\rangle = V(z)$ is the ensemble-average horizontal velocity, and average density $\langle\rho(z)\rangle = R(z)$. Here z is vertical coordinate. As a result, we have a system of two equations for the kinetic energy of turbulence $K(t,z)$ and potential energy $P(t,z)$ per unit volume. The latter is related to the density fluctuations $\langle\rho'^2\rangle$:

$$P = \frac{\langle\rho'^2\rangle \mathbf{g}^2}{2N^2R^2} \tag{1}$$

Here $\mathbf{g}$ is the gravity acceleration, $R(z)$ is defined above, and $N^2(z)$ is the squared Brunt-Väisala frequency. Note that here z-direction is chosen downwards. Under the above conditions, the general equations (18) of Ostrovsky and Troitskaya (1987)

or (6) of Gladskikh et al. (2023) are reduced to two equations for b and P:

$$\frac{\partial K}{\partial t} = V_z^2 L\sqrt{K} - N^2 L\sqrt{K}\left(1 - \frac{3P}{K}(1-G)\right) - \frac{GK^{3/2}}{L} + \frac{5}{3}\frac{\partial}{\partial z}\left(L\sqrt{b}\frac{\partial K}{\partial z}\right), \tag{2}$$
$$\frac{\partial P}{\partial t} = N^2 L\sqrt{K}\left(1 - \frac{3P}{K}(1-G)\right) - \frac{DK^{1/2}}{L}P + \frac{\partial}{\partial z}\left(\frac{L\sqrt{K}}{N^2R^2}\frac{\partial(N^2R^2P)}{\partial z}\right).$$

Here L is the outer scale of turbulence and G is the anisotropy parameter tending to 1 for strongly anisotropic turbulence with a small vertical scale compared to the horizontal scale. For details see Ostrovsky and Troitskaya (1987). Here we consider the model of locally isotropic turbulence, for which $G \sim 0.5$. The parameter L can be taken from empirical data (Rodi, 1980) or found from the turbulence spectrum (Forryan et al., 2013; Lozovatsky et al., 2006). C and D are empirical constants. The terms $CK^{3/2}/L$ and $DK^{1/2}P/L$ in (2) define the dissipation rates of kinetic and potential energy, respectively.

Before analyzing the full system (2), we note that some significant conclusions can be made from a reduced, local ODE system following from (2) after neglecting the last, diffusive terms in these equations:

$$\frac{\partial K}{\partial t} = V_z^2 L\sqrt{K} - N^2 L\sqrt{K}\left(1 - \frac{3P}{K}(1-G)\right) - \frac{CK^{3/2}}{L}, \tag{3}$$
$$\frac{\partial P}{\partial t} = N^2 L\sqrt{K}\left(1 - \frac{3P}{K}(1-G)\right) - \frac{DK^{1/2}}{L}P.$$

The coordinate z is now a parameter in these equations. In particular, they define a stationary distribution (a stable equilibrium point on the phase plane of variables b and P):

$$K_{\mathrm{st}}(z) = \frac{V_z^2 L^2}{2C} f(R_{\mathrm{i}}), \quad P_{\mathrm{st(z)}} = \frac{V_z^2 L^2}{D} - K_{\mathrm{st}} \tag{4}$$

where $R_{\mathrm{i}} = V_z^2/N^2$ is Richardson number, and

$$f(R_{\mathrm{i}}) = 1 - (4-3G)R_{\mathrm{i}} + \left[1 + R_{\mathrm{i}}^2(4-3G)^2 + R_{\mathrm{i}}(4-6G)\right]^{1/2}. \tag{5}$$

It is noteworthy that at $R_{\mathrm{i}} \to \infty$, f has a non-zero limit $f_\infty = 6(1-G)/(4-3G) > 0$ (it is 1.2 for $G = 0.5$). Hence, the turbulent energy remains finite at large Richardson numbers. General features of this solution and the turbulent Prandtl number following from it are discussed in Ostrovsky and Troitskaya (1987); Gladskikh et al. (2023). In what follows, the applicability of these simple solutions will be verified by comparison with the solutions of full equations (2). In the experiments, the dissipation rate of kinetic turbulent energy ε is commonly measured as a characteristic of turbulence. Within the semi-empirical approach, it is defined as Kolmogorov (1941):

$$\varepsilon = \frac{CK^{3/2}}{L}. \tag{6}$$

It is necessary to choose the empirical constants in the above equations and in (6). There exists a broad literature discussing these values for different laboratory and onsite conditions. In the semi-empirical models they are commonly defined by scaling. We choose the outer turbulence scale based on the results of spectral approach Forryan et al. (2013); Galperin et al. (2007),

in which the minimal wave number for the energy-carrying spectrum approximated by empirical functions is of the order of 2 cpm. Here we take $L = 0.58$ m. The range of the constant C is also wide in the literature. Since we are mainly interested in the quasi-equilibrium regime when the shear source is balanced with dissipation of turbulent energy, we use the data of Rodi (1980) to take $C = D = 0.09$. Anyway, we are mainly concerned about the order of obtained values; indeed, in the data of Forryan et al. (2013) considered below, the spread of data is up to an order.

In what follows we solve the systems (2) and (3) using the Wolfram Mathematica 13 program and compare them with each other and the data of in situ measurements.

3 Application of the local model

As mentioned, here we apply the theory to the data of three cruises described in Forryan et al. (2013). First, we digitized red curves in Fig. 2 of that paper (as mentioned, there is a large dispersion of real data, but we naturally use mean profiles). Then, using the given profiles of V_z and N_2, we calculated the Richardson number as shown in Fig. 1.

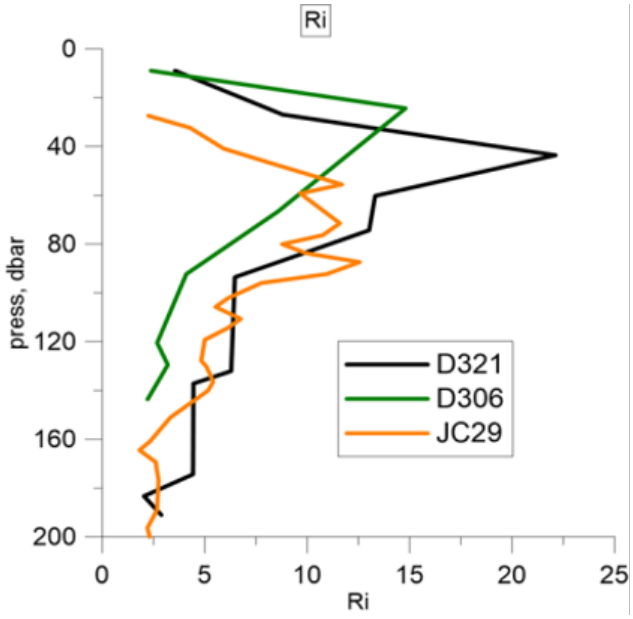

Figure 1. Profiles of Richardson number for three cruises calculated from Fig. 2 of Forryan et al. (2013) [14].

Note that for water density of 1000 kg/m^3 , static pressure in dbar coincides with depth in meters so that in our calculations we use the depth, neglecting small differences in density. As seen from Fig. 1, Richardson number exceeds 1 within all range of the available data, and its maximum lies in the range of $10 - 23$.

3.1 Cruise JC29

Now, using the interpolation of digitized data for N^2 and V_z given in Fig. 2 of Forryan et al. (2013), we solved equations (3) with the initial conditions $K(0,z) = K_0 \exp(-0.1z)$ and $P(0,z) = P_0 \exp(-0.01z)$ (we remind that in the local model, z is a given parameter). The values K_0 and P_0 varied from 10^{-6} to 10^{-5} m^2/s^2 with slight changes in transient processes but with the same asymptotic values of K and P at large times. Figure 2 shows the solutions for several depths covering the range shown in Forryan et al. (2013).

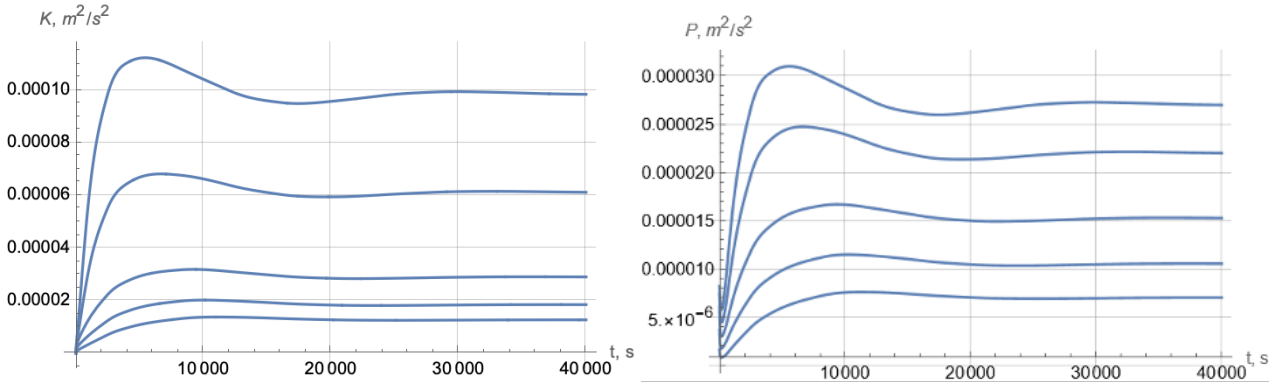

Figure 2. Temporal variation of kinetic (left panel) and potential (right panel) energy for the conditions of cruise JC29. From top to bottom: $z = 20, 30, 50, 100, 180$ m. Here $K_0 = P_0 = 10^{-6}$ m^2/s^2.

Here, the constant levels of energy are established in several hours. It is natural to use the asymptotic values for comparison with the measurement data. In the subsequent plots we use the log-lin presentation, following Forryan et al. (2013). Figure 3 shows the depth profile of the energies at large times. Note that, according to the second equation (4), the asymptotic values of P and K follow each other.

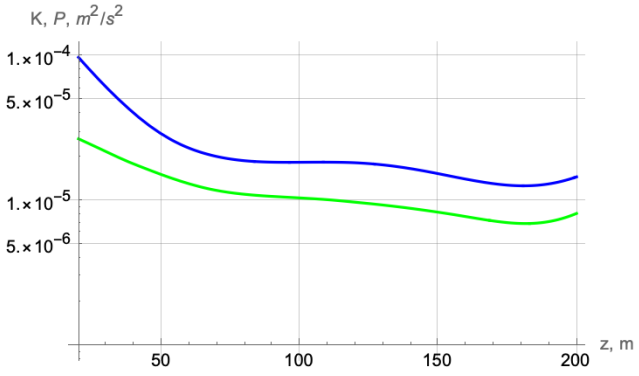

Figure 3. Profiles of kinetic (blue) and potential (green) energies for JC29 at $t = 40000$ s.

Using this solution, we calculate the turbulent dissipation rate (6) and compare it with the data of Forryan et al. (2013) after digitizing both and interpolating them by smooth functions. The result is shown in Fig. 4. Here the difference between

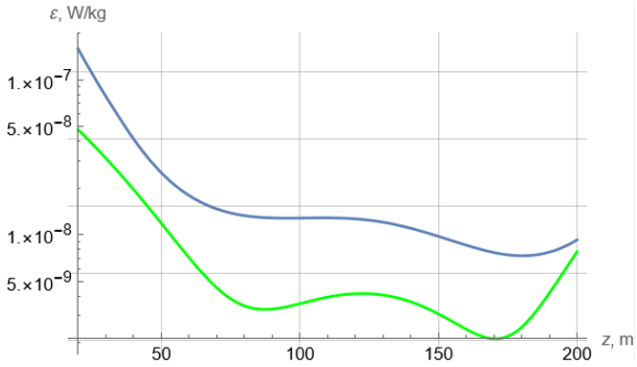

Figure 4. Profiles of turbulent kinetic energy dissipation rate for JC29. Green - interpolated data of Forryan et al. (2013) [14]. Blue - theory.

theory and measurements is mainly within a half-order. Considering the large spread of experimental data, this is a rather good agreement.

3.2 Cruise D306

To save space, for another two cruises we show only the asymptotic profiles of the corresponding values at large times. For Cruise D306, the values of kinetic and potential energies are of the same order as for JC29 (Fig. 5). Figure 6 shows the

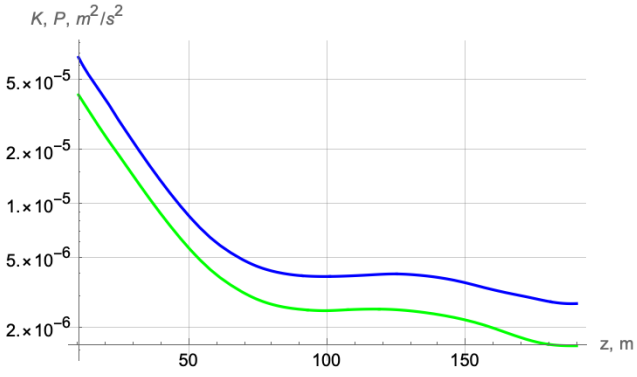

Figure 5. Profiles of kinetic (blue) and potential (green) for D306 at $t = 40000$ s.

turbulence dissipation rate. Here again the difference between theory and data of Forryan et al. (2013) is within half-order.

3.3 Cruise D321

The corresponding dependencies for cruise D321 are given in Fig. 7 and 8.

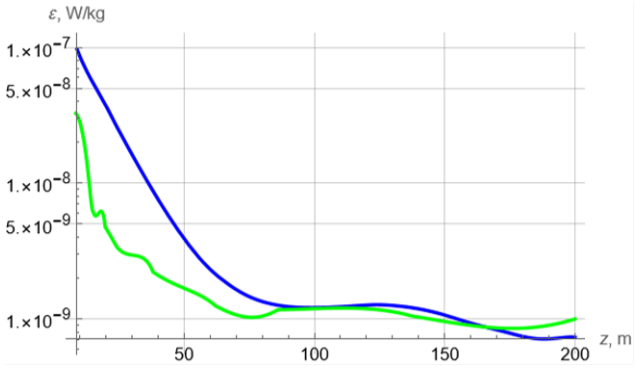

Figure 6. Profiles of turbulent kinetic energy dissipation rate for D306. Green - interpolated data of Forryan et al. (2013). Blue - theory.

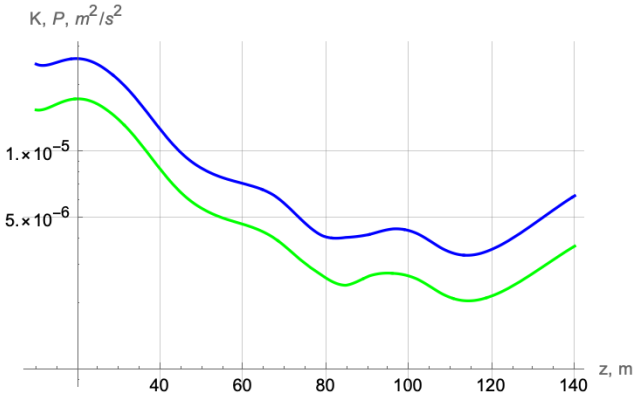

Figure 7. Profiles of kinetic (blue) and potential (green) at $t = 40000$ for D321.

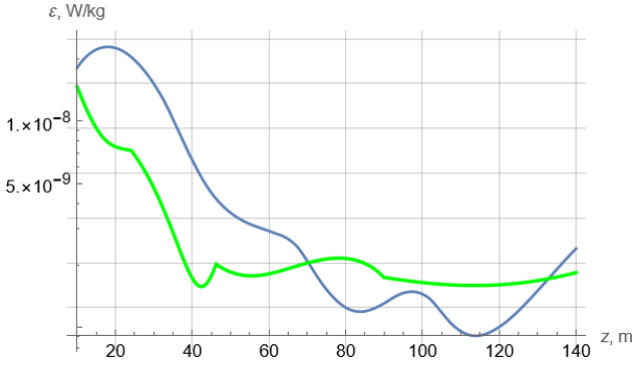

Figure 8. Profiles of turbulent kinetic energy dissipation rate for D321. Green - interpolated data of Forryan et al. (2013). Blue - theory.

Here again, one can see a good agreement between the theory and the mean measured profile.

4 Comparison with the full system

The above results were obtained in neglection of vertical turbulence diffusion. To verify this approximation, we solved the full system (2) with the same parameters and initial conditions, adding boundary conditions for fluxes of kinetic and potential energy:

$$FK = \frac{\sqrt{K}\partial K}{\partial z}, \quad FP = \frac{\sqrt{K}\partial P}{\partial z}. \tag{7}$$

They are given to be compatible with the initial conditions at initial points z_0 from which the plots start in Fig. 2 of Forryan et al. (2013), and tend to zero values at the deepest points. Then the solutions for K and P were compared with those of the local system 3. Figures below show such a comparison for the asymptotic values. In what follows, the above local solutions are shown in blue, and the solutions of equations 2 with diffusion, in orange.

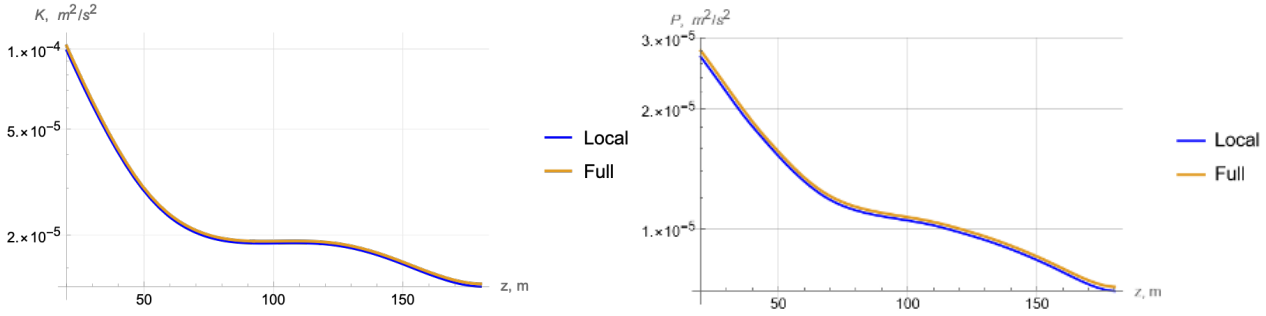

Figure 9. Cruise JC29: Comparison of profiles of kinetic (left panel) and potential (right panel) energies obtained from (3) (local) and (2) (full).

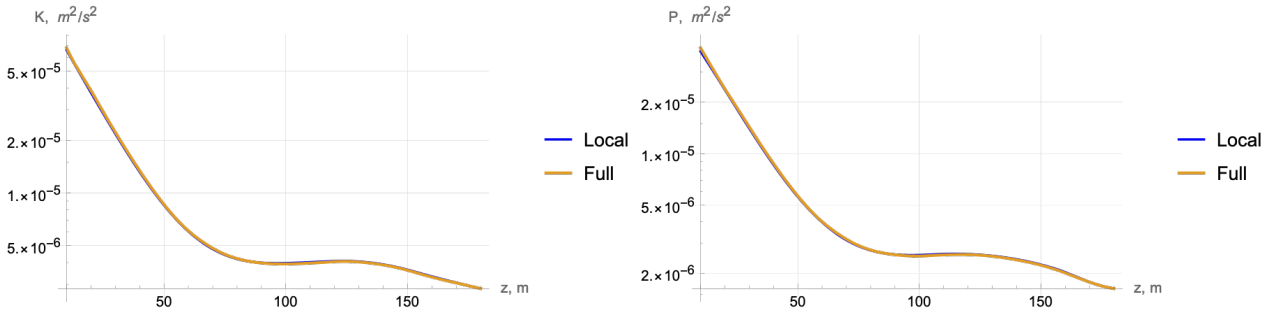

Figure 10. Cruise D306: Comparison of profiles of kinetic (left panel) and potential (right panel) energies obtained from (3) (local) and (2) (full).

In all three cases, the local and full models are practically identical. Evidently, this means the closeness of data for the dissipation rate that is a function of K. Hence, for the vertical scales of average values, vertical diffusion can be neglected, and one can use the simplified local equations (3).

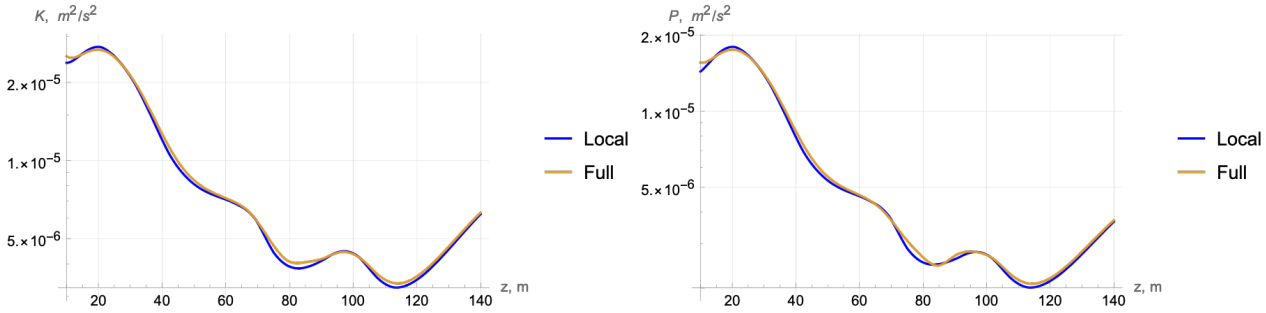

Figure 11. Cruise D321: Comparison of profiles of kinetic (left panel) and potential (right panel) energies obtained from (3) (local) and (2) (full).

5 Discussion and conclusions

In this paper we demonstrated that including the potential energy of turbulence (associated with density fluctuations in the presence of stratification) in the semi-empirical, Reynolds-type equations of a turbulent flow allows to explain the existence and evaluate the parameters of small-scale turbulence at large Richardson numbers. Application of these equations to the results of Forryan et al. (2013), where the measurements of profiles of buoyancy frequency, current shear, and dissipation rate of turbulent energy are shown together for three different areas of the ocean, provides not only qualitative but a reasonable quantitative agreement between the theory and experimental data. We have also shown that the contribution of turbulent diffusion to the level of turbulent pulsations is insignificant in the above case.

For further progress, more specific experimental data sets are desirable. Indeed, in the above calculations, we used the average data for buoyancy frequency, velocity shear, and the rate of kinetic energy dissipation plotted in red in figure 2 of Forryan et al. (2013). However, the same figure shows a significant, up to an order, data scatter from each cruise, obtained in different locations and on different days. The authors do not specify the confidence intervals of the data, and no correlation between different curves for shear and buoyancy frequency curves is known. Still, it is possible to evaluate the maximal span of results based on the extreme curves in each plot. For that, we digitized the leftmost and rightmost curves for the shear and buoyancy, interpolated them, and used the resulting functions to calculate the limits of the theoretical TKE dissipation rate using equations 4 and 5. For cruise 306 It is shown in 10.

Note that the data scattering for this value shown in Forryan et al. (2013) lies within the maximal theoretical limits which implies that knowing the real data for a specific location and time of the measurement, we would reasonably well predict the corresponding depth dependence for turbulent kinetic energy dissipation rate. Similar results take place for other cruises.

Note in conclusion that the kinetic approach used in the equations used above allows to naturally include the potential energy into consideration. Considering a large variation of empirical parameters given in different sources (Smyth et al., 2013; Liu et al., 2017; You et al., 2003), for the further study it seems important to find more of experimental data allowing to apply

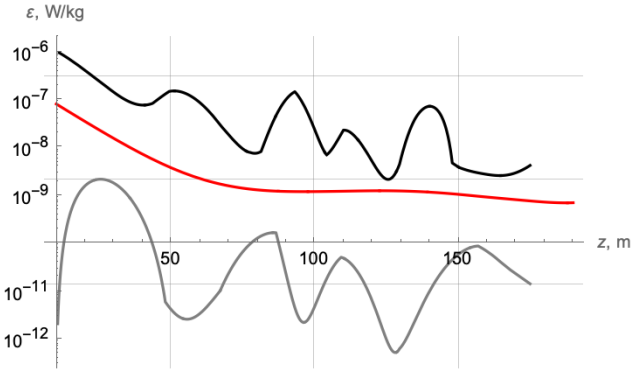

Figure 12. Maximal (black) and minimal (gray) profiles of turbulent kinetic energy dissipation rate for D306 calculated from the maximal possible scatter of data for N2 and S given in Forryan et al. (2013). Red - average value, shown in blue in 6.

the theory. We also plan to extend the present approach to description of time-varying turbulence in the field of internal waves (e.g., Moum et al., 2022).

155 *Acknowledgements.* The work was supported by the RSF project No. 23-27-00002.

References

Avicola, G., Moum, J., Perlin, A., and Levine, M.: Enhanced turbulence due to the superposition of internal gravity waves and a coastal upwelling jet, J. Geophys. Res., 112, id.C06 024, 2007.

Burchard, H.: Applied Turbulence Modelling in Marine Waters, Springer, Berlin/Heidelberg, Germany, 2002.

Burchard, H. and Bolding, K.: Comparative analysis of four second-moment turbulence closure models for the oceanic mixed layer, J. Phys. Oceanogr., 31, 1943–1968, 2002.

Forryan, A., Martin, A., Srokosz, M., Popova, E., Painter, S., and Renner, A.: A new observationally motivated Richardson number based mixing parametrization for oceanic mesoscale flow, J. Geophys. Res. Oceans, 118, 1405–1419, https://doi.org/10.1002/jgrc.20108, 2013.

Galperin, B. and Sukoriansky, S.: QNSE theory of the anisotropic energy spectra of atmospheric and oceanic turbulence, Phys. Rev. Fluids, 5, id 063 803, 2020.

Galperin, B., Sukoriansky, S., and Anderson, P.: On the critical Richardson number in stably stratified turbulence, Atmos. Sci. Lett., 8, 65–69, 2007.

Galperin, B., Sukoriansky, S., and Qiu, B.: Seasonal oceanic variability on meso-and submesoscales: a turbulence perspective, Ocean. Dynam., 71, 475–489, 2021.

Gladskikh, D., Ostrovsky, L., Troitskaya, Y., Soustova, I., and Mortikov, E.: Turbulent transport in a stratified shear flow, J. Mar. Eng. Technol., 11, 136, https://doi.org/10.3390/jmse11010136, 2023.

Hostetler, S., Bates, G. T., and Giorgi, F.: Interactive coupling of a lake thermal model with a regional climate model, J. Geophys. Res., 98, 5045–5057, https://doi.org/1029/92JD02843, 1993.

Ivanov, A., Ostrovsky, L., Soustova, I., and Tsimring, L.: Interaction of internal waves and turbulent in the upper layer of the ocean, Dynam. Atmos. Oceans, 7, 221–232, 1983.

Kolmogorov, A.: Doklady AN SSSR (in russian), 30, 299, 1941.

Liu, Z., Lian, Q., Zhang, F., Wang, L., Li, M., Bai, X., and Wang, F.: Weak thermocline mixing in the North Pacific low-latitude western boundary current system, Geoph. Res. Lett., 44, 530–539, https://doi.org/10.1002/2017GL075210, 2017.

Ljungemyr, P., N., G., and A., O.: Parameterization of lake thermodynamics in a high-resolution weather forecasting mode, Tellus A, 48, 608–621, 1996.

Lozovatsky, I., Roget, E., Figueroa, M., Fernando, H. J. S., and S., S.: Sheared turbulence in weakly stratified upper ocean, Deep-Sea Res. Pt. I, 53, 387–407, https://doi.org/10.3390/jmse11010136, 2006.

Mackay, M.: Modeling the regional climate impact of boreal lakes, Geophys. Res. Abstracts, 8, 05 405, 2006.

Mellor, G. and Yamada, T.: Development of a turbulence closure model for geophysical fluid problems, Rev. Geophys. Space Phys., 20, 851–875, 1982.

Monin, A. and Ozmidov, R.: Ocean Turbulence (in russian), Gidrometeoizdat, Leningrad, Russia, 1981.

Monin, A. and Yaglom, A.: Statisticheskaya gidromekhanika (in russian), chap. 1, Nauka, Moscow, 1964.

Moum, J., Hughes, K., Shroyer, E., Smyth, W., Cherian, D., Warner, S., Bourlès, B., Brandt, P., and Dengler, M.: Deep cycle turbulence in Atlantic and Pacific cold tongues, Geoph. Res. Lett., 49, e2021GL097 345, https://doi.org/10.1029/2021GL097345, 2022.

Ostrovsky, L. and Soustova, I.: Upper mixed layer of the ocean as a sink of internal wave energy (in russian), Okeanologia, 19, 973–981, 1969.

Ostrovsky, L. and Troitskaya, Y.: Model of turbulent transfer and the dynamics of turbulence in a stratified shear flux, Izv. Akad. Nauk SSSR, Fiz. Atmos. Okeana, 3, 101–104, 1987.

Rodi, W.: Prediction methods for turbulent flows, Hemisphere Publishing Corporation, Washington, kollmann, w. edn., 1980.

Smyth, W., Moum, J., Li, L., and Thorpe, S.: Diurnal shear instability, the descent of the surface shear layer, and the deep cycle of equatorial turbulence, J. Phys. Oceanogr., 43, 2432–2455, 2013.

Soustova, I., Troitskaya, Y., Gladskikh, D., Mortikov, E., and Sergeev, D.: A simple description of the turbulent transport in a stratified shear flow as applied to the description of thermohydrodynamics of inland water bodies, Izv. Atmos. Ocean. Phys., 56, 603–612, https://doi.org/10.1134/S0001433820060109, 2020.

Strang, E. and Fernando, H.: Vertical mixing and transports through a stratified shear layer, J. Phys. Oceanogr., 31, 2026–2048, 2001.

Stretch, D., Rot, J., Nomura, K., and Venayagamoorthy, S.: Transient mixing events in stably stratified turbulence, in: Proceedings of the 14th Australasian Fluid Mechanics Conference, Adelaide, Australia, 10-14 December 2001, pp. 625–628, 2001.

Sukoriansky, S., Galperin, B., and Staroselsky, I.: Cross-term and ε-expansion in RNG theory of turbulence, Fluid Dyn. Res., 33, 319, 2003.

Sukoriansky, S., Galperin, B., and Perov, V.: Application of a new spectral theory of stably stratified turbulence to atmospheric boundary layer over sea ice, Bound.-lay. meteorol., 117, 231–257, 2005a.

Sukoriansky, S., Galperin, B., and Staroselsky, I.: A quasi-normal scale elimination model of turbulent flows with stable stratification, Phys. Fluids, 17, id 085 107, 2005b.

Tsuang, B.-J., Tu, C.-J., and Arpe, K.: Lake parameterization for climate models, Tech. Rep. 316, Max Planck Institute for Meteorology, 2001.

You, Y., Suginohara, N., Fukasawa, M., Yoritaka, H., Mizuno, K., Kashino, Y., and Hartoyo, D.: Transport of North Pacific Intermediate Water across Japanese WOCE sections, J.Geoph. Res., 108, 3196, https://api.semanticscholar.org/CorpusID:129316495, 2003.

Zilitinkevich, S., Elperin, T., Kleeorin, N., and Rogachevskii, I.: Energy-and flux-budget (EFB) turbulence closure models for stably-stratified flows. Part I: Steady-state, homogeneous regimes, Bound.-lay. meteorol., 125, 167–191, 2007a.

Zilitinkevich, S., Elperin, T., Kleeorin, N., Rogachevskii, I., and Esau, I.: A hierarchy of Energy and Flux-Budget (EFB) turbulence closure models for stably stratified geophysical flow, Bound.-lay. meteorol., 146, 341–373, 2007b.

Appendix A: Dynamical equations for a turbulent stratified flow

Here we briefly outline the general system of equations for a turbulent stratified flow obtained in Ostrovsky and Troitskaya (1987) and developed in Soustova et al. (2020); Gladskikh et al. (2023). Without dwelling on the details which are described in these works, here we briefly outline the main points of the model. It begins by introducing the variable probability distribution function:

$$f(\boldsymbol{v}, \lambda, \boldsymbol{r}, t) = \langle \delta(\boldsymbol{u} - \boldsymbol{v}) \delta(\rho - \lambda) \rangle, \tag{A1}$$

where δ is Dirac delta-function, and the angular parentheses denote the ensemble averaging. Using this together with the Navier-Stokes equations for $\boldsymbol{u}$ and ρ, and supposing a Gaussian distribution function, the authors of Ostrovsky and Troitskaya (1987) obtained the expressions for the average fluxes of turbulent energy, momentum, and mass. They are the same as in the

common $K-\varepsilon$ theory, except for the mass flux, having the form:

$$\langle \rho' u_i' \rangle = -LV \left(\frac{\partial \langle \rho \rangle}{\partial x_i} + g_i \frac{\langle \rho'^2 \rangle}{V^2 \rho_0} - \frac{\boldsymbol{g} \beta_i}{V^2 \rho_0} \right) \tag{A2}$$

where $V = \sqrt{\langle u'^2 \rangle}$ and L, as above, is the outer scale of turbulence, g is the gravity acceleration, and β_i are the components of the vector

$$\boldsymbol{\beta} = \frac{1}{4\pi} \int d\boldsymbol{r}_1 \frac{\partial}{\partial \boldsymbol{r}} \frac{1}{\left| \boldsymbol{r} - \boldsymbol{r}_1 \frac{\partial}{\partial z_1} \langle \rho'(\boldsymbol{r}, t) \rho'(\boldsymbol{r}_1, t) \rangle \right|} \tag{A3}$$

which characterizes the effect of pressure fluctuations arising from random displacements of a particle in a stratified fluid.

The expression above for the mass flux includes the summand $g_i \frac{\langle \rho'^2 \rangle}{V^2 \rho_0} - \frac{\boldsymbol{g} \beta_i}{V^2 \rho_0}$, which, as shown below, leads to some significant differences from results obtained within the framework of known gradient models. The physical meaning of the additional terms in the expression mentioned above is related to the dependence of the force acting upon a random displacement of a liquid particle in a stratified medium on the shape of the liquid volume, namely, on the ratio of the characteristic scales L_z and L_r. As shown in Ostrovsky and Troitskaya (1987) the components of the vector $\boldsymbol{\beta}$ have the form $\beta_x = \beta_y = 0,\ \beta_z = \langle \rho'^2 \rangle R$ for a statistically homogeneous field of density fluctuations. Here R is the anisotropy parameter:

$$R \simeq \begin{cases} 1, & L_z \ll L_r, \\ \simeq \left(\frac{L_r}{L_z} \right)^2 & L_z \gg L_r, \end{cases} \tag{A4}$$

where L_z and L_r are the vertical and horizontal scales of the density field correlation, respectively.

As a result, one obtains the equations for the mean values of velocity, density, turbulent kinetic energy $K = 3V^2/2$, and variance of density pulsations $\langle \rho'^2 \rangle$:

$$\frac{\partial \langle u_i \rangle}{\partial t} + \langle u_j \rangle \frac{\partial \langle u_i \rangle}{\partial x_j} + \frac{1}{\rho_0} \frac{\partial \langle p \rangle}{\partial x_i} + g_i \frac{\langle \rho \rangle - \rho_0}{\rho_0} = \frac{\partial}{\partial x_j} \left(L \sqrt{K} \left(\frac{\partial \langle u_i \rangle}{\partial x_j} + \frac{\partial \langle u_j \rangle}{\partial x_i} \right) \right), \tag{A5}$$

$$\frac{\partial \langle \rho \rangle}{\partial t} + \langle u_i \rangle \frac{\partial \langle \rho \rangle}{\partial x_i} = 2 \frac{\partial}{\partial x_i} L \sqrt{K} \left(\frac{\partial \langle \rho \rangle}{\partial x_i} + \frac{3}{2K\rho_0} \left(g_i \langle \rho'^2 \rangle + \boldsymbol{g} \beta_i \right) \right), \tag{A6}$$

$$\frac{\partial K}{\partial t} + \langle u_i \rangle \frac{\partial K}{\partial x_i} - L \sqrt{K} \left(\frac{\partial \langle u_i \rangle}{\partial x_j} + \frac{\partial \langle u_j \rangle}{\partial x_i} \right)^2 - \frac{\boldsymbol{g}}{\rho_0} L \sqrt{K} \left(\frac{\partial \langle \rho \rangle}{\partial z} + \frac{3\boldsymbol{g}}{2K\rho_0} \left(\langle \rho'^2 \rangle + \beta_z \right) \right) + \frac{CK^{3/2}}{L} = \frac{5}{3} \frac{\partial}{\partial x_i} \left(L \sqrt{K} \frac{\partial K}{\partial x_i} \right), \tag{A7}$$

$$\frac{\partial \langle \rho'^2 \rangle}{\partial t} + \langle u_i \rangle \frac{\partial \langle \rho'^2 \rangle}{\partial x_i} - 2 \frac{\partial \langle \rho \rangle}{\partial x_i} L \sqrt{K} \left(\frac{\partial \langle \rho \rangle}{\partial x_i} + \left(g_i \langle \rho'^2 \rangle - \boldsymbol{g} \boldsymbol{\beta_i} \right) \frac{3}{2K\rho_0} \right) + \frac{DK^{1/3}}{L} \langle \rho'^2 \rangle = \frac{\partial}{\partial x_i} L \sqrt{K} \frac{\partial \langle \rho'^2 \rangle}{\partial x_i}. \tag{A8}$$

In an incompressible fluid considered here, $\nabla u = 0$. The potential energy of fluctuations is determined from the last equation because of (A8). Equations (A6) are a particular case of this system for the given average current and density stratification. In general, such effects as internal wave damping by turbulence can be included in the solution as well. On the other hand, the turbulence "breakdown" phenomenon, in which, in certain phases of the wave, the velocity shear cannot maintain a nonzero level of turbulent energy obtained using the common semi-empirical equations (Ivanov et al., 1983), does not exist here. This is also confirmed by numerical calculations using parametrization obtained based on the model above, given in the work (Gladskikh et al., 2023).